A simplified correction method for thermocouple disturbance errors in solids

A simplified correction method for thermocouple disturbance errors in solids

Ian Pope[a*], Juan P. Hidalgo[a], Rory M. Hadden[b], José L. Torero[c]

[a]The University of Queensland, School of Civil Engineering, Building 49 Advanced Engineering Building, Staff House Road, The University of Queensland, St Lucia QLD 4072 Australia
[b]The University of Edinburgh, School of Engineering, The King's Buildings, Mayfield Road, Edinburgh EH9 3DW, UK
[c]University College London, Department of Civil, Environmental and Geomatic Engineering, 104 Chadwick Building, Gower Street, London WC1E6BT, UK
*Corresponding author: Ian Pope, ian.pope@uqconnect.edu.au

Abstract:

When a thermocouple is embedded in a material of lower thermal conductivity, under certain heating or cooling conditions, the presence of the thermocouple can distort the surrounding temperature field. As a result, the measured temperatures may be very different to the 'undisturbed' temperatures that would exist without the thermocouple. This study presents the results of a sensitivity analysis of key factors influencing this thermal disturbance. A series of heat transfer models and accompanying experiments are used to demonstrate the effects of thermocouple geometry, contact conditions, thermal properties, and heating regime on the temperature measurement error. These tailored finite element models were validated against experiments on vermiculite insulation board, which confirmed the accuracy of the models in simulating the thermal disturbance for inert heating conditions. Also, a simplified version of the finite element model was used to calculate the thermal disturbance error for a number of conditions, and subsequently to predict a range of corrected temperatures for the experimental measurements. This correction method was found to greatly improve the accuracy of the results for inert heating conditions. Since the method does not account for the effects of moisture in heat transfer, a creep of uncorrected errors could be observed.

Keywords: thermocouple; temperature measurement; heat transfer; thermocouple error; error correction; fire

Nomenclature:

a	absorptivity
C_P	specific heat capacity
E	error
h	heat transfer coefficient
k	thermal conductivity
$\dot{m}''$	mass flux
$\dot{q}''$	heat flux
r	radius from TC centre
t	time
T	temperature
x	Distance from heated surface

Greek letters:

α	thermal diffusivity
ε	emissivity
ρ	density
σ	Stefan-Boltzmann constant

Subscripts:

c	convection
corr	corrected
condens	condensation
e	external
evap	evaporation
g	of the gas
(Hot)	'high' temperature
Inc	Inconel
l	losses
net	net
O2	oxygen
p	pyrolysis
r	radiation
s	surface
TC	thermocouple
un	undisturbed
V	vermiculite
vap	vapour
w	water
∞	ambient

1. Introduction

As the various stakeholders in the construction industry try to balance competing financial, social, and environmental interests, there is a continual drive for innovation. In order to satisfy these criteria, novel construction materials and systems of increasing complexity are being introduced, for which conventional design frameworks may not be applicable. In particular, fire safety frameworks have failed to keep pace with the introduction of new combustible or bio-based building materials, and non-conventional structural systems – leading in some cases to catastrophic consequences.

In order to quantify and predict the fire performance of these building elements, their thermo-mechanical response to fire exposures is defined through appropriately tailored experimentation or standardised test methods. One of the most important components of these experiments is the in-depth temperature profile measurement, which provides insight into the physical and chemical processes occurring within the material, and is critical in validating predictive thermal and thermo-mechanical models. There are numerous examples of this approach in studies across a wide range of materials, such as timber [1,2], insulation materials [3], and swelling intumescent coatings [4]. In addition to their use in providing information to modellers, internal temperature measurements are routinely used on their own as a quantitative metric or failure criteria in fire safety research and standard testing.

Fire testing standards globally impose critical temperature criteria for specific measuring points within the tested components, on external surfaces, or at the interface between different components [5,6] – particularly to indicate conditions relevant to the onset of pyrolysis, a risk of ignition, or loss of structural capacity. Temperature measurements for components of a prototype under Standard Fire Test [5] conditions may also be used to calculate the Fire Resistance Level that would be achieved by a corresponding building element [6].

Beyond the application to fire research and testing, in-depth temperature measurements under much lower heat exposures may be used to analyse the thermal performance of building assemblies, including calculation of the "R-value" [7]. Moreover, in-depth temperatures are often used in inverse modelling of well-defined materials to calculate the heat flux on an exposed surface, or to estimate material properties when the heat flux is known. This method is often applied in fire research [3,8,9], but is also widely used in manufacturing, industrial processes, and thermal engineering. A commonality of all these applications is the significant difference between the overall thermal conductivity of the thermocouple and that of the substrate [7]. In all of these cases, accurate measurement of internal temperatures is essential.

Thermocouples of various designs are ubiquitous in research and standard testing due to their durability, versatility, and ability to operate over a wide range of temperatures. While there is a wide range of thermocouple types available, the basic design comprises two narrow wires of different metals that meet at a junction where the actual temperature measurement is taken. These wires are otherwise separated from each other by some kind of electrically insulating material, generally powdered aluminium oxide (Al_2O_3) or magnesium oxide (MgO). The wires and insulation may then be encased in fibreglass or a metal sheath, depending on the durability required, with the junction exposed or also contained within. The ensemble of these features will define the overall thermal properties of the thermocouple.

1.1 Thermocouple disturbance errors and correction methods

There are a number of potential errors inherent to the use of thermocouples for solid-phase temperature measurement, depending on the characteristics of their implementation. In

particular, when a thermocouple with a relatively high thermal conductivity (k) is embedded in a material of much lower conductivity, this can induce a disturbance in the temperature field around the thermocouple due to a 'thermal bridging' effect [10]. This causes the material surrounding the thermocouple tip – where the temperature is measured – to be cooled relative to the undisturbed material, as heat diffuses more easily along the thermocouple. As a result, the measured temperatures within the material (T_{TC}) may be much lower than the 'undisturbed' temperatures (T_{un}) that would exist without the presence of the thermocouple. This effect has been recognised in fire research [1,11,12], but much of the work in quantifying or correcting the error has been developed in the context of industrial applications such as metal casting [13], water quenching [14], and nuclear engineering [15]. Beck [10] described this phenomenon for the case of a thermocouple – represented as a solid cylinder – embedded perpendicular to the heated surface in a material of lower thermal conductivity. Through this analytical study, Beck found that this temperature disturbance can be very significant when the thermal properties of the thermocouple are not close enough to those of the surrounding material. In certain cases, the temperature disturbance ($T_{un} - T_{TC}$) was found to exceed 50 % of the undisturbed temperature rise ($T_{un} - T_{\infty}$) for the early transient heating period. Beck defined the problem in terms of a series of non-dimensional parameters, of which the most critical was the ratio of conductivities, K, followed by the ratio of the products of density (ρ) and specific heat capacity (C_P) of each material, C:

$$K = \frac{k}{k_{TC}} \qquad \text{and} \qquad C = \frac{\rho C_P}{(\rho C_P)_{TC}}$$

Beck developed a method to predict and correct the measurement error for this specific geometry [10,15], but with a number of simplifying assumptions. In addition to the idealisation of the thermocouple as a homogeneous cylinder, Beck assumed perfect thermal contact with the surrounding material, which was taken to be a semi-infinite body. At some point ahead of the thermocouple tip, a plane normal to the thermocouple is heated by a heat flux that is time-variable but constant in space. Behind the heated plane, thermal properties must remain constant with temperature, and only inert heat conduction through the thermocouple and embedding material is considered. This method of correcting measured temperatures, which is described in detail by Beck [10,15] and more recently by Woolley and Woodbury [13], involves a numerical inverse convolution procedure to find a correction kernel function that can be used to predict the undisturbed temperatures. Firstly, the transient heat transfer problem is solved numerically for a constant arbitrary surface heat flux, in order to produce a set of artificial values for T_{TC} and T_{un}. These simulated temperatures are then used in the inverse convolution to compute the correction kernel values. If material properties remain constant, then the correction kernel function is independent of the variation in surface heat flux over time [13], so the correction can be calculated without prior knowledge of the true time-variable surface heat flux. Finally, these correction kernel values are used in the forward convolution to predict the real T_{un} from the measured T_{TC}.

While this method is effective, and has been demonstrated successfully for relatively simple materials and geometries [13], its applicability in fire testing is limited by its simplifying assumptions. For example, assuming perfect thermal contact may be unrealistic in practice, where internal thermocouples are typically inserted into holes drilled into a material or assembly. Due to the practical constraints of machining tolerances and material imperfections, there is likely to be a contact resistance or small air gap between the thermocouple and embedding material. The assumption of a uniform surface heat flux is also challenged in many fire testing scenarios, particularly when measurements are needed close to the heated surface

of more complex materials or assemblies. In these cases, the heat transfer interactions between the tested components, thermocouples, and the external conditions, may be highly non-uniform. Finally, modelling inert heat conduction with constant thermal properties is often inappropriate for the high thermal loads relevant to fire testing. Under high heat fluxes, many materials of interest undergo physical and chemical processes, such as pyrolysis, swelling, shrinking, cracking, and mass transport, which can affect the internal thermodynamics. The relationships between a thermocouple, its embedding material, and the external boundary conditions, are summarised in Fig. 1.

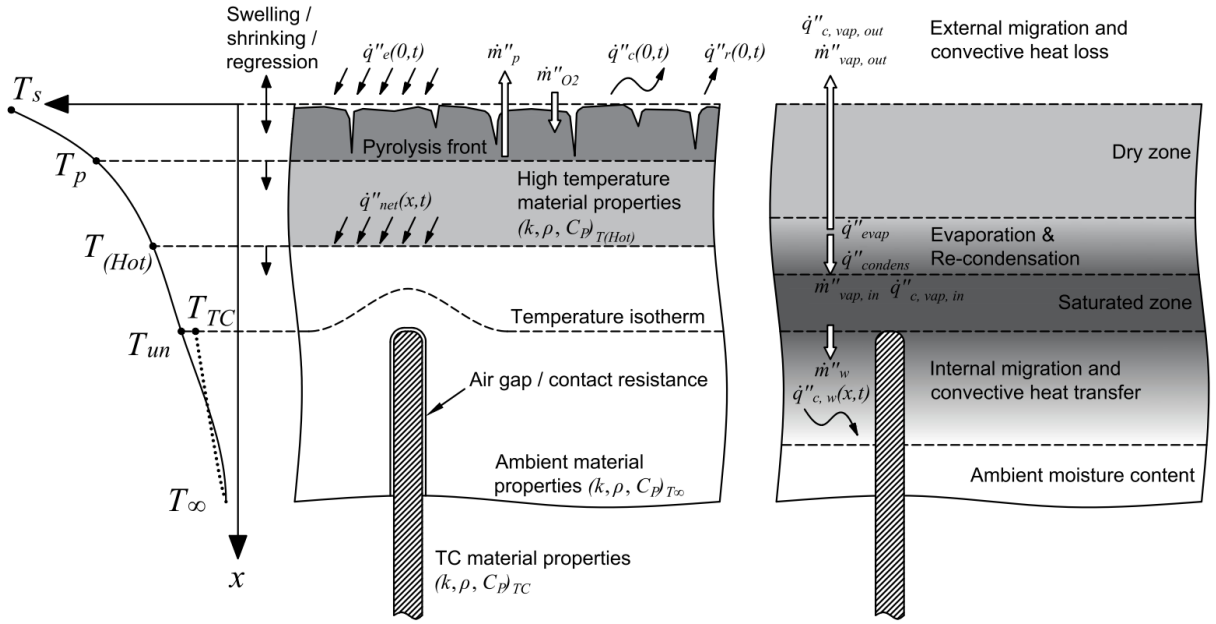

Fig. 1. Summary of key phenomena that can influence temperature measurements and proposed correction methods for a thermocouple inserted perpendicular to the heated surface. Typical boundary conditions, as well as chemical and physical changes are described on the left, with the specific effects of moisture migration, evaporation and re-condensation shown on the right.

As shown in Fig. 1, the externally applied heat flux $\dot{q}''_e(0,t)$, convective heat loss $\dot{q}''_c(0,t)$, and radiative heat loss $\dot{q}''_r(0,t)$ contribute to the exposed surface boundary condition, and all may vary with space and time. The surface itself may shift due to swelling, shrinking, cracking, or ablation of the substrate. Chemical and physical changes in the substrate can substantially change its thermal properties, and may present additional heat sources or sinks. Many materials undergo pyrolysis and oxidation reactions, involving the transport of pyrolysates ($\dot{m}''_p$), and oxygen ($\dot{m}''_{O2}$). The boundary of pyrolysing material is often approximated by an isotherm at a critical temperature (T_p). Even below this temperature, where changes in the chemistry and geometry of the substrate are negligible, there may be changes in the thermal properties (k, ρ, C_P) above ambient temperature. Although these are generally continuously temperature dependent properties (TDP), they are often discretised as constant values between specific temperature ranges. These may include an ambient properties zone, where temperatures are close to ambient (T_∞), and a region of high temperature thermal properties, which may be delineated by the pyrolysis temperature (T_p) or some other temperature above which the properties change significantly above ambient ($T_{(Hot)}$). When the conductivity of the thermocouple (k_{TC}) is higher than that of the surrounding material, there will be a depression in the temperatures around the tip of the thermocouple, such that the actual temperature measured by the thermocouple (T_{TC}) is lower than the undisturbed temperature (T_{un}) existing at the same

depth (x_{TC}) far away from the thermocouple. Beck's correction method [10,15] is limited to measurements taken behind a plane subjected to a net heat flux $\dot{q}''_{net}(x,t)$, in front of which all of these complex processes may occur, but behind which only inert heat diffusion and constant thermal properties are accounted for.

Fig. 1 also describes several effects that the presence of moisture can have in a porous medium under a high heating rate, including endothermic evaporation, mass transfer, convective heat transport, and re-condensation [16,17]. While these phenomena actually occur in a continuous manner through the volume, they are represented simply here as fluxes imposed across discrete boundaries. As the heat wave progresses through the substrate, it evaporates and frees bound water, resulting in an endothermic heat sink (simplified as a heat flux $\dot{q}''_{evap}$). This forces some of the initial moisture out via the surface of the material ($\dot{m}''_{vap,\ out}$) with an associated loss of sensible heat ($\dot{q}''_{vap,\ out}$), while some of the vapour travels deeper into the material ($\dot{m}''_{vap,\ in}$) where it recondenses, transferring both sensible heat and the latent heat of vaporisation ($\dot{q}''_{vap,\ in}$, $\dot{q}''_{condens}$). Eventually, if the moisture content and heating rate are high enough, a saturated layer may build up as the pores of the substrate fill. This has been observed for concrete, in which a growing saturated layer can form a 'moisture clog' between the dried layer and inner regions at ambient moisture content [16,18,19]. The region of higher than ambient moisture content gradually moves deeper, transporting a mass flux of water ($\dot{m}''_{w}$) that alters the effective local thermal properties and heats up the surrounding material through convection ($\dot{q}''_{c,\ w}(x,t)$). These phenomena are particularly troublesome for correction methods, because they occur at relatively low temperatures – up to ~100 °C – and absorb large enthalpies, which means that they may have an important effect at significant distances from the heated surface of a material. Furthermore, when moisture migration and accumulation in-depth is possible, these effects may increase in severity with distance behind the heated surface as the layer of elevated moisture content grows [16,18,19]. Crucially, since these phenomena are strongly temperature dependent and transient, they cannot be accounted for in a model without well-defined material properties and representative boundary conditions. This is a limitiation of generalised correction methods such as Beck's [10], which cannot account for temperature dependent behaviours.

Given the limitations in correcting the thermocouple temperature disturbance for a material with complex behaviour, Beck [10] recommended inserting thermocouples parallel to the heated surface, in order to minimise the thermal bridging effect near the tip. While this configuration has been shown to reduce the thermal disturbance significantly [12,13], there is still an appreciable effect, which is dominated by the heat capacity ratio, C [20]. Nevertheless, fire testing standards state that internal temperatures should be measured by taking the thermocouple wires along an isotherm for a distance of at least 50 mm from the junction "where possible", with no additional correction advised [5]. This requirement is often unfeasible for tested systems unless the thermocouple is installed during assembly – a restriction for independent investigation. There are significant practical constraints when positioning thermocouples parallel to the heated surface of a pre-fabricated sample, particularly for large-scale experimentation. If the thermocouple can only be inserted via a drilled hole, it may be impossible to drill a sufficient distance in from the sample side, such that the measurement point is at the desired position, while this may be achieved easily by drilling from the back. Moreover, drilling parallel to the heated surface even on a small scale can result in significant error in the actual distance of the end of the hole from the heated surface. As demonstrated by Reszka [1], a misalignment in the drilling angle of only 5 ° over a length of 50 mm can result in an error in the distance from the heated surface of 4.4 mm when drilling from the side, compared with 0.2 mm from the back.

For laminated timber, Farhni *et al.* [11] recommend only inlaying thermocouples between lamellae, parallel to the heated surface. Aside from the need to install the sensors during fabrication, this severely constrains the locations at which thermocouples can be positioned, particularly when the thickness of lamellae is large. Terrei *et al.* [21] also studied this problem for wood, and proposed a solution for small-scale experiments, in which the sample is cut in half and thin wire thermocouples are inlaid in machined grooves between the two re-joined halves of the sample. This approach was seen to greatly reduce the temperature disturbance, but it is only feasible for small samples that can be altered in this way. An additional complication for thermocouples installed parallel to the heated surface – whether inserted into a drilled hole or inlaid – is that the location of these sensors may change over time if the material surrounding them shrinks or swells under heating. A thermocouple perpendicular to the heated surface may not be disturbed as easily by a swelling or shrinking front traversing the embedding material.

1.2 Proposed simplified correction method

Considering the practical constraints and additional sources of error associated with installing thermocouples parallel to a heated surface, it is worthwhile developing a simplified method of correcting thermocouple disturbance errors that can be applied more broadly in fire research. This thermocouple disturbance error will be referred to as $E(x,t)$, which can be defined as a percentage by the ratio of the absolute temperature disturbance to the undisturbed temperature rise above ambient, as given by Eq. (1).

$$E(x,t) = \frac{(T_{un}(x,t) - T_{TC}(x,t))}{(T_{un}(x,t) - T_{\infty})} \tag{1}$$

If the error history of a thermocouple is known, the experimentally measured thermocouple readings can then be 'corrected' simply by rearranging Eq. (1) and solving for $T_{un}(x,t)$. This is simple enough for a well-defined experimental setup, where a heat transfer model can be constructed to calculate the error using material properties and heating conditions that are known *a priori*. However, in most practical scenarios, either the heating conditions or the variation with time of the temperature-dependent thermal properties of the components may be unknown or poorly defined. These uncertainties may be effectively addressed through sensitivity analyses that bound the relevant parameters.

As observed in previous work by the authors [12], the exact magnitude of the net heat flux at the surface does not have a direct effect on the percentage error ($E(x,t)$) when material thermal properties are constant. Rather, the relative change in the net heat flux in space and time affects the evolution of the resulting error curve. This is analogous to the Beck correction method, in which the correction kernel function is insensitive to the real value of the surface heat flux [10,13,15]. Generally, the net heat flux on a surface exposed to fire conditions will not remain constant or uniform, but will vary as a function of heat losses from radiation and convection as the surface temperature rises, and with the evolution of the applied heat flux. In many cases, the evolution of the net surface heat flux is unknown – particularly when the surface temperature is likewise unknown. This knowledge gap can be addressed through sensitivity cases that bound the possible variations in net heat flux. Since the precise magnitude of the net heat flux is not required, the external heat flux ($\dot{q}''_e$) can be given an arbitrary constant value of 1 kW/m^2 in these sensitivity cases. When a thermocouple is close to the surface, the induced disturbance decreases the local surface temperatures in such a way that the surface heat losses ($\dot{q}''_l$) can be highly non-uniform. At the same time, many boundary conditions common in fire experimentation, such as convective heating or cooling, tend to promote a uniform surface

temperature. A uniform temperature across the heated surface will incur the minimum thermal disturbance from the thermocouple, while a uniform net heat flux will induce the maximum disturbance [10]. With a constant external heat flux, a case of minimal heat losses ($\dot{q}_l'' \approx 0$) will approach the uniform net heat flux scenario, while a high heat loss case will approximate uniform surface temperature. For simplicity, surface heat losses are linearised in this sensitivity analysis, and the heat transfer coefficients for radiation (h_r) and convection (h_c) combined into a total heat loss coefficient (h_l):

$$\dot{q}_l'' = h_c(T_s - T_\infty) + \varepsilon\sigma\left(T_s^4 - T_\infty^4\right) = h_c(T_s - T_\infty) + h_r(T_s - T_\infty) = h_l(T_s - T_\infty) \qquad (2)$$

This total heat loss coefficient can be varied between a 'low heat loss' (LHL) value and a 'high heat loss' (HHL) value. These sensitivity cases are applicable to scenarios in which a material is undergoing continuous heating, approaching a steady state.

In addition to the variation in the net surface heat flux, the thermal disturbance is governed by the material properties of the different components (reflected by *K* and *C*), and their geometries. While the geometries of the thermocouple and the hole are expected to be known within a small error margin, the evolution of temperature-dependent thermal properties over time may not be. This may also be addressed through a sensitivity analysis, by modelling a range of constant thermal properties for each of the components, associated with different temperature ranges. This is the approach used by Woolley and Woodbury [13] in their application of Beck's correction method.

The proposed correction method involves the application of this sensitivity analysis to an inert heat transfer model that incorporates the specific geometry of the thermocouple and embedding materials. Using the artificial boundary conditions and material properties of the sensitivity analysis, a series of error histories can be calculated, which can directly be used with the experimentally measured temperatures (T_{TC}) to predict a range of corrected temperatures (T_{corr}). As with Beck's method, phenomena that change the geometry of the substrate, or which provide additional heat sources or sinks, cannot be accounted for once they reach the depth of the thermocouple. However, this method is mathematically simpler than the previous correction methods, and allows for consideration of variable surface heat fluxes. Calculation of *E(x,t)* from the heat transfer model also allows a more realistic representation of the interactions between the thermocouple, its hole, and the embedding material, since these can each be represented as separate components.

This study presents an experimental and modelling examination of the factors influencing the thermal disturbance error and the proposed correction method. The experimental investigation is carried out for the heating of vermiculite insulation board, a relatively simple and well-defined material that is commonly used in fire experimentation and industrial processes. Vermiculite is a porous material, with a small equilibrium moisture content under ambient conditions. The effects of this moisture are not accounted for in the models, but their impact will be observed in the experiments for comparison. This work builds upon an initial study by the authors [12] that characterised the error for a charring material and applied an earlier iteration of the correction method. This correction was much more limited, in that it applied only for low temperatures (before the onset of charring) and did not account for variability in thermal properties or boundary conditions. The validation of the improved method presented in this paper provides a basis for its application to materials with more complex behaviour in future studies.

2. Experimental materials and methods

A series of experiments were conducted in order to explore the sensitivity of the thermocouple disturbance error to a range of practical variables. In these experiments, samples of vermiculite insulation board were subjected to constant radiant heat fluxes of either 5 or 60 kW/m^2 from a Mass Loss Calorimeter [22] for 20 minutes. These heat fluxes were chosen to replicate thermal boundary conditions that are representative of potential fire exposures. Moreover, each heat flux will induce distinct ranges of temperature-dependent thermal properties in the component materials. The samples, with dimensions of 90 × 90 × 50 mm, were oriented vertically, with the radiant heat flux applied horizontally on one face as shown in Fig. 2. The vertical orientation was chosen to allow thermocouples to be easily inserted via either the back or side of the sample, without being obstructed by the sample holder on the bottom surface. All sides of the sample except the exposed face were covered with ceramic paper insulation and reflective aluminium tape, to block irradiation of the sides of the sample and to minimise heat losses. This insulation was also used to shield the external part of the thermocouples from radiation.

Holes were drilled in either the back or side of the sample to allow the insertion of thermocouples either perpendicular or parallel to the heated surface. For simplicity, thermocouples that are inserted parallel to the heated surface are often referred to as 'side-inserted' thermocouples throughout this paper, while thermocouples oriented perpendicular to the heated surface are called 'back' or 'rear-inserted' thermocouples. These holes were drilled such that the tips of the thermocouples would be either 3 or 20 mm from the exposed surface. The holes were drilled with either a uniform diameter, with a small air gap surrounding the thermocouple along its entire inserted length, or with a stepped diameter, such that the final 9 mm of the hole had the same diameter as the thermocouple. The 9 mm distance was chosen because it allowed a tight fit to be achieved around the tip of the thermocouple, without the friction becoming too great to fully-insert it. For the side-inserted thermocouple case (parallel to the heated surface), holes were drilled 45 mm into the side of the sample in a staggered arrangement, as shown in Fig. 2. For rear-insertion (perpendicular to the heated surface), holes were drilled in a circle of 20 mm radius, such that there was at least 20 mm separation between the centrelines of each thermocouple. The thermocouples used in each experiment were either 1.0 mm or 1.5 mm in diameter, with holes drilled to a diameter of either 1.5 mm or 2.0 mm depending on the tightness of fit to be achieved.

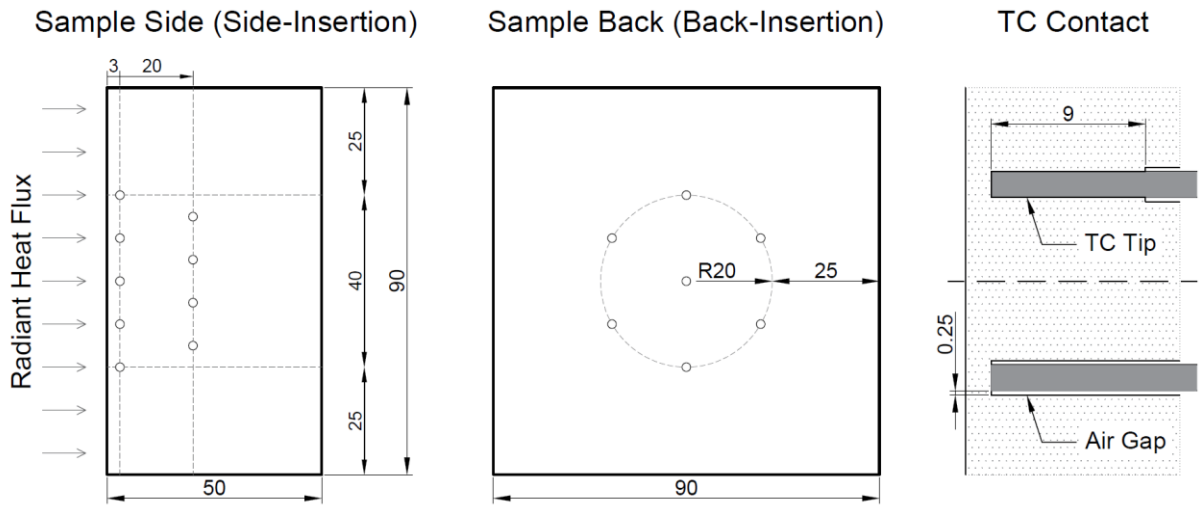

Fig. 2. Placement of thermocouples in tested samples in each orientation, with different tip contact conditions (dimensions in mm).

Mineral-insulated metal-sheathed type K thermocouples with insulated junctions were used to measure the temperatures at each depth within the samples. These were composed of chromel and alumel thermocouple wires, surrounded by magnesium oxide powder insulation within an Inconel 600 sheath. One thermocouple was dissected, so that the dimensions of the sheath and wires could be measured. From these measurements, the relative sizes of the cross-sectional areas of each component of the thermocouple were calculated in proportion to the total thermocouple area. These cross-sectional fractions of 55 % for the sheath, 41 % for the MgO, and 4 % for the wires, were then used to calculate weighted-average values for the conductivity and density of the thermocouple from the individual material properties shown in Fig. 3. Since the exact MgO density was unknown, the properties of MgO with a solid volume fraction of 65 % have been used in this calculation as a sensitivity case, since the conductivity of 98 % dense MgO is relatively similar to that of Inconel 600. A weighted-average value for heat capacity was calculated based on the relative mass fractions of each component. Due to the incomplete data for chromel and alumel at elevated temperatures, the 4 % fractional area of the wires was also assigned the properties of Inconel 600 when calculating the weighted-average properties for this sensitivity case. This is a reasonable approximation since the area of the wires is so small, and the properties of chromel and alumel are close to those of Inconel at the temperatures for which data is available. The properties of the vermiculite board are also shown in Fig. 3. The moisture content of the vermiculite was 1.1 % by mass, measured by weighing a reference sample before and after drying it for three days in an oven at a temperature of 103 °C.

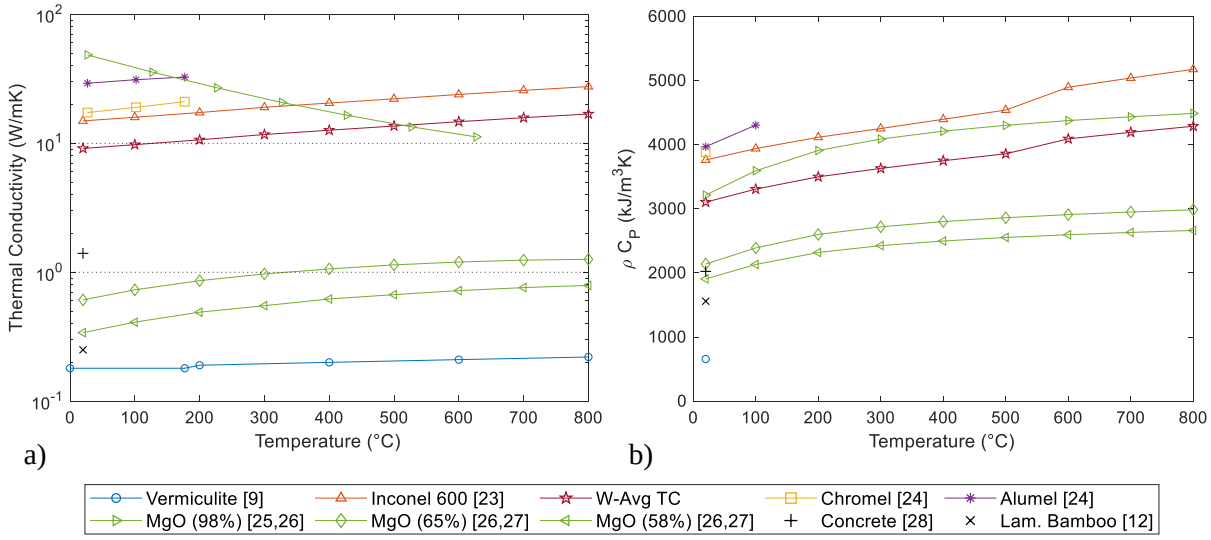

Fig. 3. Thermal conductivities and ρC_P values of thermocouple components and embedding materials over relevant temperature ranges from [9,12,23–28].

As noted in Section 1.1, there is often an error in the placement of the end of a hole drilled parallel to the heated surface due to slight misalignment of the drilling angle. To limit the impact of this error, all samples that had thermocouples inserted from the side were cut in half at the end of the experiment, so that the actual position of the end of the hole relative to the heated surface could be measured. The maximum error in the location of the centreline of a hole was found to be approximately 1.3 mm, corresponding to an error in the drilling angle of approximately 1.6 ° for a 45 mm hole. The results of any thermocouples found to have been in holes with a placement error of more than 0.75 mm were discarded, and the distances of the remaining holes from the heated surface were averaged for each experiment. This average

distance is presented along with the average temperature measurements throughout Section 4. Despite the omission of results from some misplaced thermocouples, at least three valid measurements were recorded for all of the experimental cases. The matrix of experiments and models in Table 2 details the specific combination of variable conditions in each case.

3. Modelling approach

Each of the experiments was replicated with finite element heat transfer models using the commercial software Abaqus and ANSYS. These models were specifically tailored to the experimental conditions in each case, so that they could be directly compared with the experimental measurements. The purpose of this exercise was to validate the accuracy of the models in simulating the thermal disturbance created by a thermocouple, so that the models could be further applied to investigate the sensitivity of this disturbance to a greater range of variables.

Models were run both with and without a thermocouple (and hole) present, so that the 'disturbed' thermocouple temperatures and 'undisturbed' vermiculite temperatures could be calculated. The models were based on an inert heating regime, with no internal mass transfer, heat generation, or internal radiation, but allowing for temperature dependent thermal properties. This is described by a simplified form of the *heat diffusion equation*, Eq. (3), for the general three-dimensional heating case.

$$\frac{\partial}{\partial x}\left(k\frac{\partial T}{\partial x}\right)+\frac{\partial}{\partial y}\left(k\frac{\partial T}{\partial y}\right)+\frac{\partial}{\partial z}\left(k\frac{\partial T}{\partial z}\right)=\rho C_P\frac{\partial T}{\partial t} \tag{3}$$

For the cases in which a thermocouple was inserted perpendicular to the heated surface, a two-dimensional axisymmetric model was created in Abaqus with the axis of rotational symmetry along the centreline of the thermocouple, as shown in Fig. 4 a). For the side-insertion case, a three-dimensional model incorporating the entire sample block and thermocouple was created, as shown in Fig. 4 b). The three-dimensional model was constructed in ANSYS, since more powerful computational resources were available for use with this software. Abaqus and ANSYS are widely used FEM software, and are well validated for inert heat transfer.

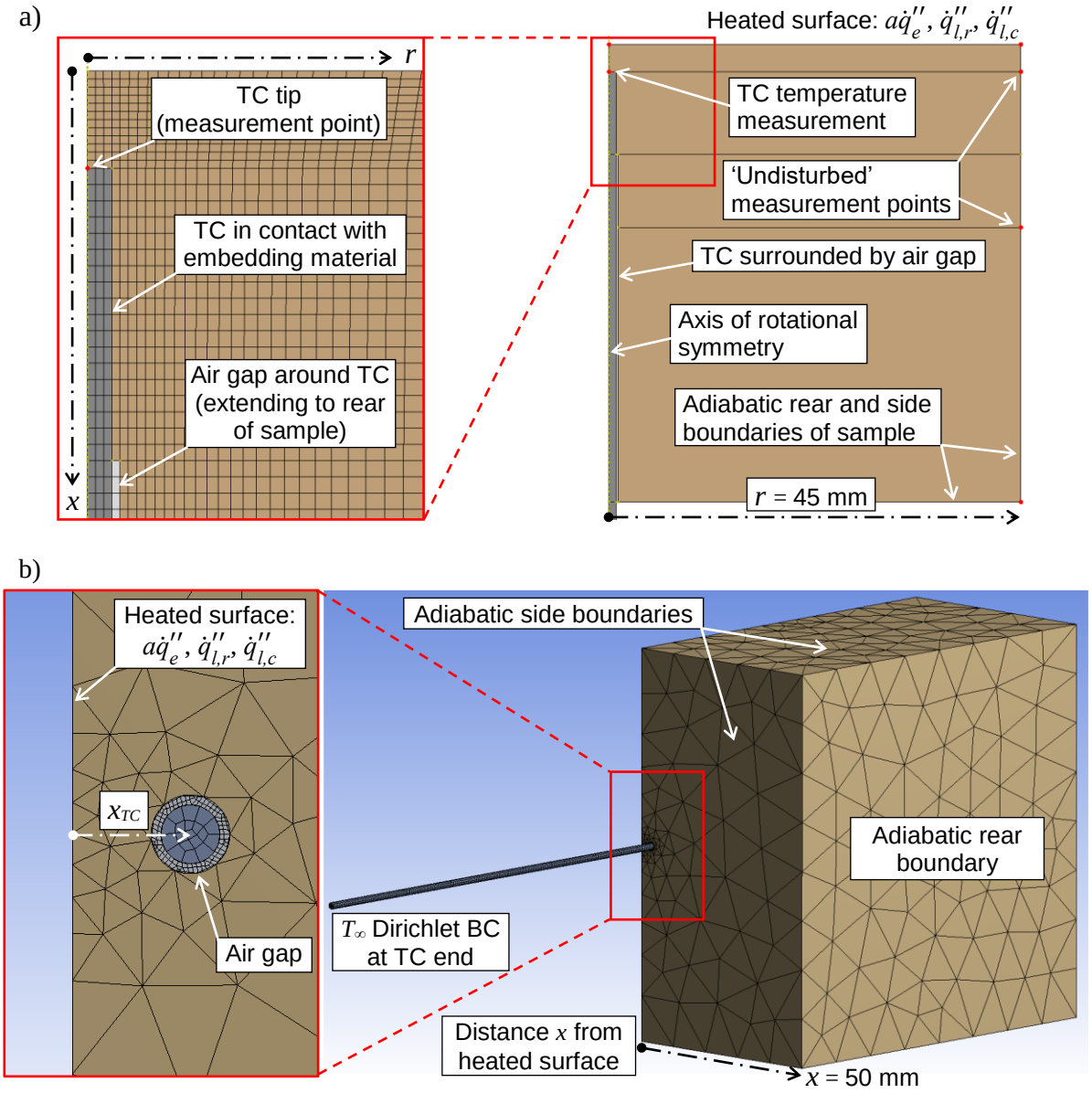

Fig. 4. a) 2D axisymmetric Abaqus model of a thermocouple (TC) inserted from the rear of the sample, and b) 3D ANSYS model of thermocouple inserted from the side of the sample.

A uniform external heat flux, $\dot{q}_e''$, replicating the irradiation from the cone heater, was applied on the heated surface of the vermiculite, along with convective and radiative cooling. The terms of the net heat flux on the heated surface are detailed in Eq. (4). Since vermiculite is opaque, in-depth radiation was neglected and radiation was treated purely as a surface phenomenon [9,28]. Thus, the net heat flux was imposed as a boundary condition on the exposed elements.

$$\dot{q}_{net,\,s}'' = a\dot{q}_e'' - \dot{q}_{l,r}'' - \dot{q}_{l,c}'' = a\dot{q}_e'' - \varepsilon\sigma\left(T_s^{\,4} - T_\infty^{\,4}\right) - h_c(T_s - T_\infty) \qquad (4)$$

The convective heat transfer coefficient, h_c, is dependent on the Nusselt number, Nu, as well as the conductivity of the gas, k_g, and the characteristic length of the sample, L, as shown in Eq. (5) [29].

$$h_c = \frac{\overline{Nu} \cdot k_g}{L} \tag{5}$$

Due to the vertical orientation of the heated surface, the space-mean value of the convection coefficient was calculated from the empirical correlation for the Nusselt number, as shown in Eq. (6), developed by Churchill and Chu [29] for laminar free convection over a vertical plate. This correlation is applicable for this experimental regime since the Rayleigh number, $Ra < 10^9$, and the surface of the sample is approximately isothermal, due to the near uniformity of the imposed heat flux and the insulation of the side boundaries. The characteristic length was taken as 0.09 m, the vertical length of the heated surface.

$$\overline{Nu} = 0.68 + \frac{0.670 Ra^{1/4}}{[1 + (0.492/Pr)^{9/16}]^{4/9}} \tag{6}$$

Where the Rayleigh number, *Ra*, and Prandtl number, *Pr*, are given by:

$$Ra = \frac{g\beta(T_s - T_\infty)L^3}{\nu\alpha} \qquad \text{and} \qquad Pr = \frac{\nu}{\alpha}$$

In which the acceleration due to gravity, g, and the characteristic length, L, are constant, while the inverse of the film temperature, $\beta = T_f^{-1}$, the kinematic viscosity of the air, ν, and the thermal diffusivity of air, α, vary with the film temperature, $T_f = (T_s + T_g)/2$ [9,28,30].

The side and rear boundaries of the vermiculite were modelled as adiabatic, as they were covered in ceramic paper insulation in the experiments. These same boundary conditions were also imposed in the 3D model, except that the externally applied heat flux was attenuated away from the centre, based on a heat flux mapping of the cone heater. As a result, the imposed surface heat flux beyond the central 30 mm radius was reduced by 7.5 % for the nominal 5 kW/m^2 exposure, and by 5 % for a central heat flux of 60 kW/m^2.

A thermocouple length of 150 mm was included in both 2D and 3D models, with the far end of the thermocouple maintained at a constant ambient temperature. In reality, the thermocouple wires (if not the sheath) will continue much further than this, but it is impractical to extend the modelled control volume beyond this point. The assumption of an ambient temperature Dirichlet boundary condition at a distance of 103-120 mm beyond the outer surface of the embedding material is a reasonable simplification, considering the length of thermocouple outside of the embedding material that is exposed to ambient temperatures. This simplification also provides an upper bound to the prediction of energy conducted away from the tip by the wires. In the rear-insertion model, convective and radiative heat losses from the surfaces of the thermocouple where it extends beyond the rear face of the sample were neglected. This simplification was made to the 2D axisymmetric model because the very small Biot number of the thermocouple ($Bi << 1$) means that heat losses from radiation and convection will be negligible in comparison to the heat conducted along the thermocouple. For the 3D side-insertion model, the temperature of the thermocouple where it exits the sample is much higher than for the rear-insertion case, so radiative and convective cooling was included on the exposed surface. The value of the Nusselt number for convective cooling of the exposed portion of the thermocouple was calculated from the correlation presented by Churchill and Chu [31] for free convection on a horizontal cylinder:

$$\overline{Nu} = \left\{0.60 + \frac{0.387Ra^{1/6}}{[1 + (0.559/Pr)^{9/16}]^{8/27}}\right\}^2 \quad (7)$$

For the 2D axisymmetric model, a structured quadrilateral mesh of quadratic elements was applied, with elements ranging in size from 0.25 to 2 mm along the radial axis and from 0.25 to 1 mm from the front to the back faces. Due to the geometry of the side insertion case, a free mesh of quadratic tetrahedral and hexahedral elements was used to create the 3D model, based on the adaptive meshing solution provided by the ANSYS software. The adequacy of the mesh in either case was verified through a sensitivity study that found convergence in the model output close to the value provided by the base model. When the number of elements was approximately doubled, the temperature at the tip of a thermocouple 3 mm from the heated surface differed by less than 0.1 °C for the 2D model, and less than 0.2 °C for the 3D model.

In each of the models, there is a degree of uncertainty around the thermal properties designated to the various thermocouple components, and their interactions with each other and the embedding material. While the properties of the Inconel sheath is well characterised, the conductivity of the magnesium oxide insulation depends greatly on the packing density of this powder, as seen in Fig. 3, which is difficult to establish post-fabrication. Furthermore, the thermal contact resistances between each of the wires, insulation, sheath and embedding material are unknown, and these values are typically only obtained through inverse modelling. As a simplification, the thermocouple has been implemented in most of the model cases as a solid cylinder with uniform material properties. In the simplest case, the properties of Inconel 600 have been applied to the entire cylinder, since the sheath comprises the majority of the cross-section, and these thermal properties are similar to those of the chromel and alumel wires. Sensitivity cases were also modelled, in which the weighted-average properties of the sheath and insulation (with a 65 % solid volume fraction) were applied to the entire thermocouple cross-section. This was also compared with a model in which the sheath and insulation were individually represented in the geometry, with their respective thermal properties. In all cases, contact resistance has been neglected, and perfect contact has been assumed between the thermocouple and the embedding material. Where there is an air gap between the thermocouple and the hole, only conduction through the air has been accounted for, with convection and radiation neglected.

The temperature dependent properties of conductivity, density, and specific heat capacity assigned to the vermiculite, Inconel 600, magnesium oxide, and the weighted-average thermocouple material are given in Fig. 3. The thermal properties of air from Incropera and DeWitt [28] were used for the air gap surrounding the thermocouple, and to calculate the convection conditions on the heated vermiculite surface and the external part of the thermocouple.

The radiative properties of the exposed vermiculite surface were determined based on an earlier study of the same material from Laschütza [9]. Following the approach of Boulet *et al.* [32], the total absorptivity of the vermiculite corresponding to the radiant spectral emission from the cone heater – approximated by a black body – was found to be 0.89 for an incident heat flux of 5 kW/m^2 and 0.75 for 60 kW/m^2. While Laschütza provides temperature dependent total emissivity data, the model software only allowed for a single constant value. Since radiation is most significant at higher temperatures, these inputs were estimated for each incident heat flux based on the highest experimental temperature measurements from thermocouples inserted parallel to the heated surface at a depth of 3 mm. Consequently, emissivity values of 0.91 and 0.80 were selected for external heat fluxes of 5 and 60 kW/m^2, respectively.

A summary of the boundary conditions applied for each of the 2D and 3D models – tailored to the specific experimental conditions – is provided in Table 1, while Table 2 outlines the different combinations of variables applied to each of the model cases.

Table 1. Tailored model properties and boundary conditions

Input parameter	2D model (rear insertion)		3D model (side insertion)	
$\dot{q}_e''$ Incident radiation	Uniform over heated surface		Mapped heat flux distribution	
	5 kW/m^2	60 kW/m^2	4.6 - 5 kW/m^2	57 - 60 kW/m^2
T_∞ Ambient temperature	26 °C	26 °C	28 °C	25 °C
Vermiculite (sample surface):				
a_V Absorptivity	0.89	0.75	0.89	0.75
ε_V Emissivity	0.91	0.80	0.91	0.80
$h_{c,V}$ Convective heat transfer coefficient	Empirical relationship for a hot vertical plate in quiescent air [29]			
Sample rear BC	Adiabatic		Adiabatic	
Sample side BC	Adiabatic		Adiabatic	
Inconel 600 (thermocouple length external to sample block):				
ε_{Inc} Emissivity	N/A	N/A	0.7	0.7
$h_{c,Inc}$ Convective heat transfer coefficient	N/A	N/A	Empirical relationship for a hot horizontal cylinder in quiescent air [31]	
TC external end BC	Dirichlet boundary condition at T_∞			
Mesh	Quadratic, quadrilateral Elements: 6089 - 6116 Nodes: 19007 - 19044		Quadratic, tetra/hexahedral Elements: 51916 - 61249 Nodes: 227648 - 240870	

Table 2. Tailored models simulating real conditions in experiments on vermiculite

TC Orientation	Heat Flux (kW/m^2)	Diameter (mm)	TC Tip Contact	TC Properties	Model/Experiment Name
Back					
(2D model)	5	1.5	Perfect for 9 mm	Inconel only	[B1] Back-5-1.5-Inc-TDP
				Weighted-average	[B2] Back-5-1.5-WAvg-TDP
				Inconel and MgO	[B3] Back-5-1.5-MgO-TDP
Experiment				–	*Back-5-1.5-Exp*
	60	1.5	Perfect for 9 mm	Inconel only	[B4] Back-60-1.5-Inc-TDP
				Weighted-average	[B5] Back-60-1.5-WAvg-TDP
				Inconel and MgO	[B6] Back-60-1.5-MgO-TDP
Experiment				–	*Back-60-1.5-Exp*
	60	1.5	Air gap around tip	Inconel only	[B7] Back-60-1.5-Gap-TDP
Experiment				–	*Back-60-1.5-Gap-Exp*
		1.0			[B8] Back-60-1.0-Gap-TDP
Experiment				–	*Back-60-1.0-Gap-Exp*
		0.5			[B9] Back-60-0.5-Gap-TDP
		2.0			[B10] Back-60-2.0-Gap-TDP
	5	0.5	Air gap around tip	Inconel only	[B11] Back-5-0.5-Gap-TDP
Side					
(3D model)	5	1.5	Perfect for 9 mm	Inconel only	[S1] Side-5-1.5-Inc-TDP
				Weighted-average	[S2] Side-5-1.5-WAvg-TDP
				Inconel and MgO	[S3] Side-5-1.5-MgO-TDP
Experiment				–	*Side-5-1.5-Exp*
	60	1.5	Perfect for 9 mm	Inconel only	[S4] Side-60-1.5-Inc-TDP
				Weighted-average	[S5] Side-60-1.5-WAvg-TDP
				Inconel and MgO	[S6] Side-60-1.5-MgO-TDP
Experiment				–	*Side-60-1.5-Exp*

4. Results and discussion

4.1 Evaluation of thermal disturbance

Results from both the models and experiments presented in this section clearly show the disturbance induced by a thermocouple when embedded in a material of much lower conductivity. This is particularly significant when the thermocouple is inserted from the "back", i.e. perpendicular to the heated surface.

4.1.1 Model comparison and validation

In all cases, the models predicted that the temperature at the tip of a rear-inserted thermocouple would be significantly lower than the undisturbed temperature that would exist if no thermocouple was present. This temperature difference is greatest during the transient heating period, but persists even as a quasi-steady state is reached. In both the models and experimental results, the temperatures at the tip of the side-inserted thermocouples were higher than for the rear-insertion case, and were much closer to the predicted undisturbed temperatures. The undisturbed temperature predictions from the 2D axisymmetric Abaqus model matched very closely with those from near the centreline of the 3D ANSYS model.

Fig. 5 displays the results for cases in which a 1.5 mm diameter thermocouple is inserted into a hole with perfect contact between the thermocouple and surrounding vermiculite for 9 mm nearest to the tip. Temperature histories are shown for the undisturbed case, in which no thermocouple is present, as well as cases where a thermocouple is represented by a solid cylinder of Inconel 600, or as a cylinder with the weighted-average thermal properties of Inconel 600 and magnesium oxide (65 % solid fraction). The cases in which the Inconel thermocouple sheath and MgO core are each included separately (B3, B6, S3, S6) have not been shown in these graphs, since this was found to produce very similar results to the case with weighted-average thermal properties – with a maximum difference of 4.5 °C for 60 kW/m^2 irradiation. This supports the proposition that weighted-average thermal properties can be used to simplify the more complex geometries and interactions between the individual thermocouple components [10]. Similarly, the results of the weighted-average thermocouple properties cases have not been included for the side-insertion cases in Fig. 5 c) and d) for visual clarity, since these results were so close to those of the solid Inconel cases. Experimental measurements (Exp) are presented as averages for each depth, with standard deviation intervals shaded. For the side-inserted thermocouple experiments, the actual average distance between the centrelines of the thermocouple tips and the heated surface is stated on Fig. 5 c) and d).

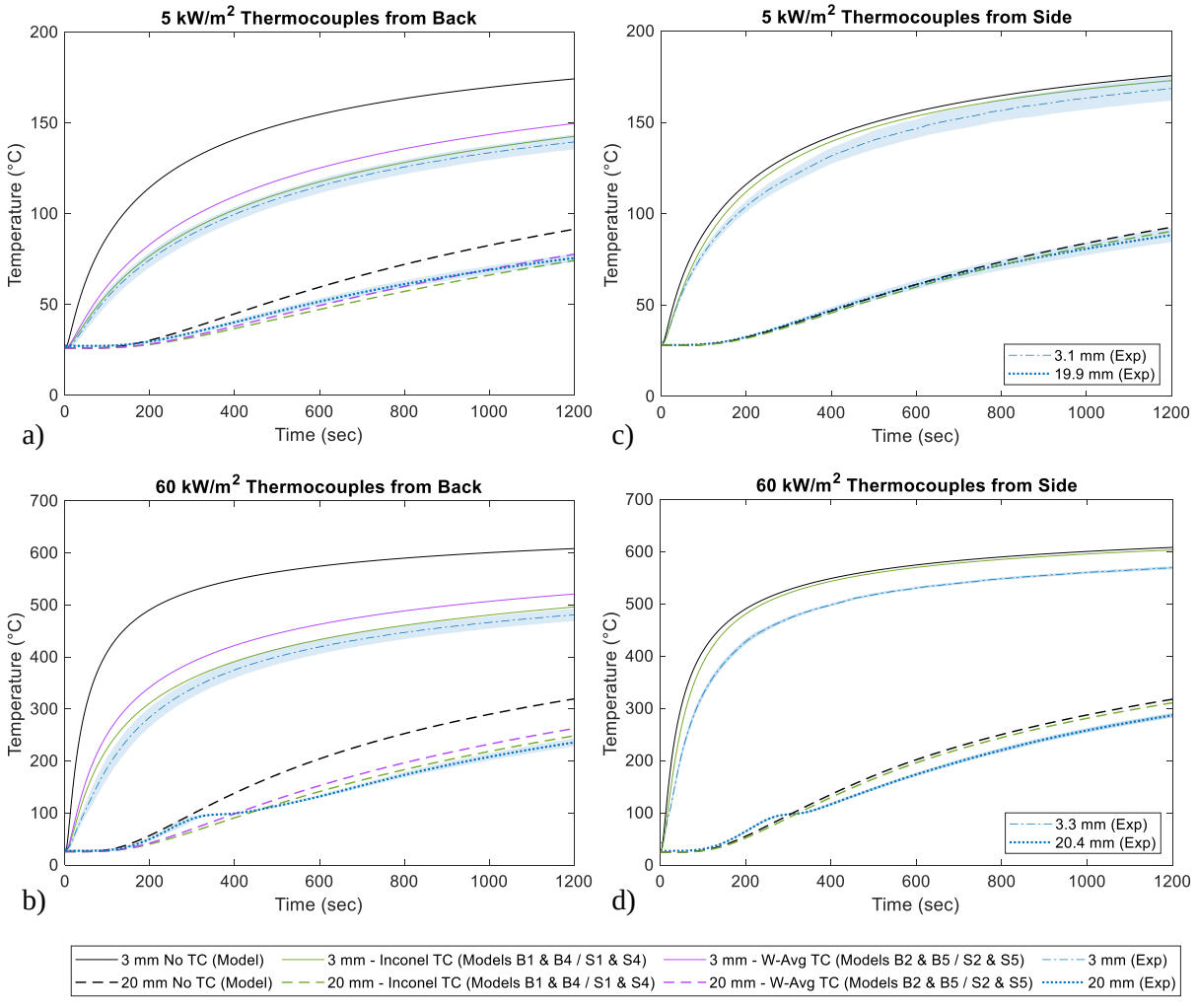

Fig. 5. Modelled and experimental temperature histories for thermocouples inserted from the back or side. Thermocouples are assigned the thermal properties of either solid Inconel or a weighted-average of Inconel and MgO (65 % solid volume fraction). Standard deviation intervals are shaded for experimental results.

The very low variability (maximum standard deviation of 7.5 °C) in the experimental results shown in Fig. 5 d) is due to greater consistency in the placement of the thermocouples in this experiment. When the locations of the thermocouple tips were measured following the experiment, all of the thermocouples that were nominally intended to be placed at a depth of 3 mm were found to be actually at a depth of 3.3 mm. In comparison, the depths of the corresponding thermocouples in the experiment shown in Fig. 5 c) ranged between 2.8 mm and 3.3 mm. Therefore, while the average depth is more accurate for the experiment in Fig. 5 c), the higher consistency in placement of thermocouples for the experiment in Fig. 5 d) results in a lower variability of temperature measurements.

From observation of the experimental results for thermocouples at a depth of 20 mm, it is apparent that the heat transfer within the vermiculite samples is not truly inert. This is most obvious in the 60 kW/m^2 heating cases, where the temperature measured by the 20 mm thermocouple initially exceed model predictions, before reaching a plateau at around 100 °C. This effect is almost certainly due to the presence of moisture within the porous vermiculite, which was not accounted for in the model. While the relatively small 1.1 % moisture content is not sufficient to produce a significant effect close to the heated surface, as the heat wave travels through the material and forces some of the moisture to migrate inwards it accumulates at greater depths [16–19]. The migration of this moisture creates an additional convective heat transfer effect, as the hot moisture equilibrates with the relatively cooler surroundings ahead. This would explain the faster than predicted temperature rise up to 100 °C seen for the 20 mm depth in all cases. The other implication of this moisture accumulation is that approaching 100 °C there is a temperature plateau due to the endothermic effect of evaporation. This plateau is likely to become more pronounced with depth, due to the accumulation of moisture and the lower conduction heat flux. This is particularly evident in Fig. 5 b) and d) for 60 kW/m^2 irradiation, but it may also explain why the slope of the experimental temperature histories at 20 mm decrease faster than expected as they approach 100 °C in the 5 kW/m^2 irradiation cases.

Aside from the effect of the moisture, which is outside the scope of this study, the experimental results for rear-inserted thermocouples match quite well with the model predictions for a solid Inconel thermocouple. The model predictions for a thermocouple with the weighted-average properties of Inconel and MgO (with a solid fraction of 65 %) are always higher than those for solid Inconel – due to the lower weighted-average conductivity, as shown in Fig. 3. This weighted-average thermocouple model (B2, B5), and the model with a discrete MgO core (B3, B6), appear to overestimate the measured temperatures. This is likely due to the actual solid volume fraction of the MgO being significantly greater than 65 %. The conductivity of MgO powder increases greatly as the solid volume fraction increases from 65 % to 98 %, so any powder with a density towards the upper end of this range will have a conductivity in the same order of magnitude as that of Inconel 600. This explains why the pure Inconel thermocouple model (B1, B4) provides a closer prediction of the experimental results.

As shown in Fig. 5 c) and d), the experimental measurements from thermocouples inserted parallel to the heated surface are slightly lower than those predicted by the models, particularly for the higher heat flux. This is partly due to the fact that the real measured distances of the thermocouple tips were slightly further than 3 mm from the heated surface. However, this alone does not fully explain the discrepancy between the modelled and experimental results. Possible explanations are that the thermal properties implemented for either the vermiculite or thermocouple materials do not quite match reality, or that the modelled radiative and convective boundary conditions are not totally representative. Another likely explanation is that the contact conditions between the thermocouple and the vermiculite are not adequately characterised, due to the unquantified contact resistance between these components. Nevertheless, the results

overall suggest that the experimental conditions are represented quite well in the models (apart from moisture effects), particularly for rear-insertion.

Fig. 5 clearly illustrates the influence of the thermocouple orientation on the measured temperature results. At both heat flux exposures, the experimental and model results for side-inserted thermocouples are significantly higher than those for rear-inserted thermocouples at each depth. When comparing the mean experimental temperatures in the 60 kW/m^2 exposure case shown in Fig. 5 b) and d), it can be seen that the measurements from side-inserted thermocouples at an average depth of 3.3 mm are up to 143 °C higher than those of the rear-inserted thermocouples at 3 mm after 150 seconds. Even after 1200 seconds, as a quasi-steady state is approached, this gap is 88 °C. The corresponding gap in predictions from modelled thermocouples for these times at a depth of 3 mm are 170 °C and 107 °C, respectively.

4.1.2 Sensitivity of disturbance to thermocouple geometry

Fig. 6 examines the effects of different a) thermal contact conditions and b) diameters on thermocouples inserted perpendicular to the heated surface. In Fig. 6 a), experimental and model results are presented for the case of a thermocouple inserted into a hole with a tight fit for the first 9 mm from the tip, as well as a case where there is a small gap along the entire length of the thermocouple. For the model of the "9 mm Contact" case (B4), perfect thermal contact is implemented between the vermiculite and the thermocouple over this length, with conduction across the 0.25 mm air gap for the remainder of the hole. In the second "Air Gap" model (B7), perfect contact between the vermiculite and thermocouple is assumed only at the end of the modelled thermocouple cylinder.

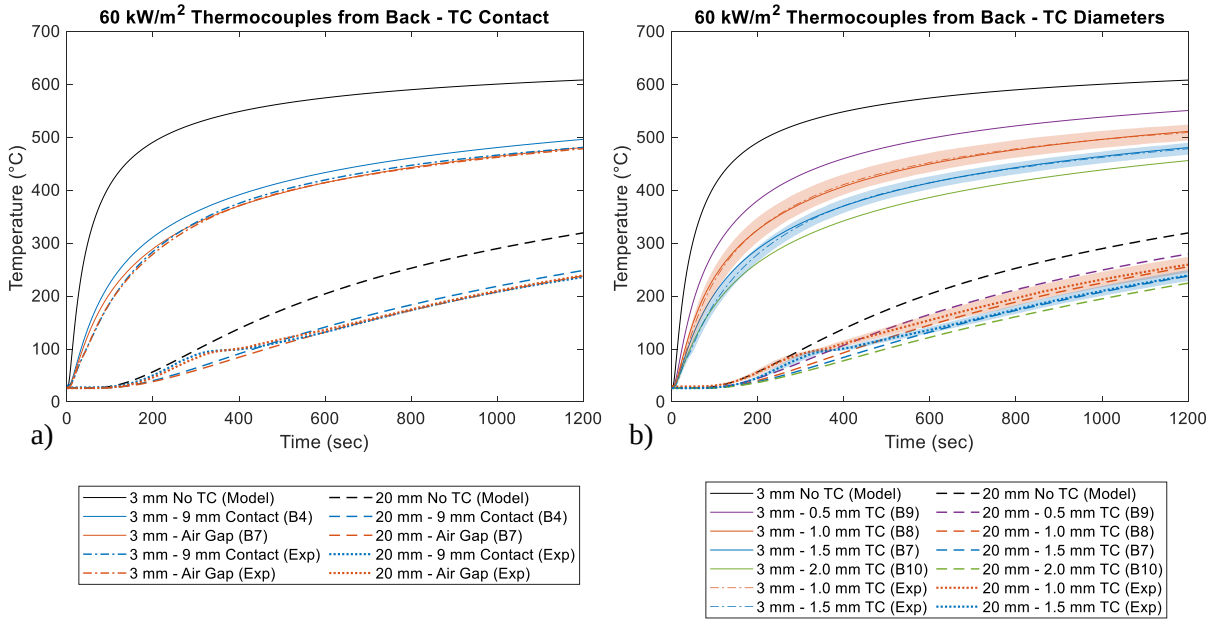

Fig. 6. Effect of thermocouple a) contact conditions, and b) diameter on temperatures measured by a rear-inserted thermocouple.

Model results reflect the impact of thermal contact efficiency, with higher temperatures predicted when there is perfect contact between the thermocouple and the embedding material than when there is an air gap surrounding the full length of the thermocouple. However, this effect is not clearly seen in the experimental results, for which the average temperatures measured in each case are almost identical (standard deviation intervals have been omitted for

visual clarity). Instead, the experimental measurements for both geometries almost exactly match the model predictions for the case with a consistent air gap along the length of the hole. This is likely due in part to the previously mentioned omission of contact resistance between the thermocouple and the embedding material. In reality, even a thermocouple inserted into a hole of equal diameter will not conduct heat perfectly with the surrounding material, due to ridges and bumps on each surface creating additional air gaps [28]. As such, it is likely that the model of a thermocouple surrounded by an air gap for its full length (B7) is a more realistic representation of both experimental conditions. This approach of modelling a small air gap around the thermocouple represents a useful technique for bounding the impact of contact resistance when it is difficult to quantify explicitly, but this should be evaluated on a case-by-case basis.

In Fig. 6 b), model results for thermocouples of 0.5, 1.0, 1.5 and 2.0 mm diameter are presented, along with experimental results for 1.0 and 1.5 mm diameter thermocouples. In all of the model and experimental cases, there is a 0.25 mm air gap around each thermocouple for the full embedding length. Experimental results fit very well with the model predictions for this configuration, which together show how thermocouple diameter affects the temperatures recorded. A thermocouple of smaller diameter has less capacity as a thermal bridge to disturb the surrounding temperature fields in the embedding material, since the energy conducted along the thermocouple will be proportional to its cross-sectional area. For the models presented, the 0.5 mm thermocouple is predicted to reduce the thermal disturbance error significantly when compared with a 1.5 mm diameter thermocouple. Nonetheless, even a 0.5 mm diameter thermocouple, which may be the smallest that can practically be used, is predicted to measure temperatures that are still significantly lower than T_{un}. For the 3 mm depth under 60 kW/m^2 irradiance, this difference is predicted to reach a maximum of 123 °C in the first 90 seconds, before approaching a quasi-steady difference of around 57 °C.

4.2 Error correction

When analysing the magnitude of the thermal disturbance in each case, the predicted and experimentally measured thermocouple temperatures must be compared with an undisturbed reference value, T_{un}. This reference value has been taken to be the temperature of the embedding material at each depth as calculated by the Abaqus model with no thermocouple (or hole) present. It must be acknowledged that there is an uncertainty associated with this, as the undisturbed temperature is controlled by the accuracy of the model, and cannot be experimentally determined. This is the underlying problem that this study is addressing, as it can be seen that even measurements from thermocouples inserted parallel to the heated surface will carry some error – whether due to misplacement or a smaller thermal-bridging effect. For these reasons, the experimental results from side-inserted thermocouples have not been used as reference temperatures for the purpose of quantifying errors, but they are useful as a qualitative benchmark. Despite this uncertainty, the accuracy of this simple model in predicting the experimentally measured results suggests that these undisturbed temperature predictions are close to reality – aside from the effects of the moisture at lower temperatures. Using this reference, the measurement error of a thermocouple can then be calculated as a proportion of the rise in temperature above ambient predicted for the undisturbed case, as shown in Eq. (1).

The correction method described in Section 1.2 has been applied to the experimental results of the rear-inserted thermocouples shown in Fig. 5 a) and b). In this process, sensitivity cases are selected to bound the range of possible values for thermal properties and external boundary conditions. The total heat loss coefficient from Eq. (2) is varied between a ‘low heat loss’ (LHL) value of 10 W/(m^{2}K) and a ‘high heat loss’ (HHL) value of 80 W/(m^{2}K), which respectively

correspond to near-ambient and high (~800 °C) surface temperatures in this experimental configuration. These heat loss conditions were combined with an arbitrary constant external heat flux of 1 kW/m^2 to constitute the thermal boundary conditions for the sensitivity cases.

In the scenarios examined in this study, two cases bound the spectrum of possible values for the conductivity ratio, *K*, which could be present during different stages of heating. Firstly, the 'ambient properties' case (Amb), in which all material properties are kept constant at their ambient temperature values. This is most representative of the earliest stage of heating, when the thermocouple and the surrounding material are yet to heat up significantly, or when the imposed heat flux is low and temperatures do not rise significantly above ambient. Secondly, an upper bound value for *K* results from the 'high temperature material properties' case (Hot), where the thermal properties of the embedding materials are taken to be their values at 700 °C, but the thermocouple properties remain at their ambient levels.

By running the simple 2D axisymmetric model with different combinations of inputs from the extreme cases described above, a range of possible error evolutions was computed from the model temperature outputs for a 1.5 mm diameter thermocouple. These sensitivity cases are outlined in Table 3.

Table 3. Sensitivity case models with linearised heat losses and constant thermal properties

TC Orientation	Heat Losses	Diameter (mm)	TC Tip Contact	Material Properties	Model Name
Back (2D model)	'Low' 10 W/(m^{2}K)	1.5	Perfect for 9 mm	Ambient Inconel and Vermiculite	[C1] Back-LHL-1.5-Amb
				Ambient Inconel, "Hot" Vermiculite	[C2] Back-LHL-1.5-Hot
	'High' 80 W/(m^{2}K)	1.5	Perfect for 9 mm	Ambient Inconel and Vermiculite	[C3] Back-HHL-1.5-Amb
				Ambient Inconel, "Hot" Vermiculite	[C4] Back-HHL-1.5-Hot

The error curves calculated from these sensitivity models are bounded by two extreme cases. The highest errors predicted are for the 'ambient properties' case with low heat losses (C1), while the lowest predicted thermal disturbance error results from the 'hot vermiculite properties' case with high heat losses (C4). The errors calculated for each of these cases are shown in Fig. 7, along with the errors calculated by the high fidelity models (B1, B4) presented in Table 2 that include the true external heat fluxes, heat losses, and temperature-dependent thermal properties. Despite the range in thermal properties and heating conditions, the predicted errors for each thermocouple depth remain relatively close, with the two extreme cases differing by less than 10 % at any given time.

As would be expected, the sensitivity case with constant ambient temperature properties and relatively low surface heat losses (C1) closely approximates the error predictions from the 5 kW/m^2 external heat flux model, since the maximum material temperature predicted by this realistic case is only 191 °C at the surface. The error curve predicted by the 60 kW/m^2 external radiation model (B4) is bounded on the lower side by the other extreme of a model with hot vermiculite properties and relatively high surface heat losses (C4). The 'hot vermiculite properties' case becomes less appropriate at greater depths, as the temperature of the vermiculite near the thermocouple tip is much lower than that assumed for this model. Nevertheless, the application of these sensitivity cases – which required only details of the

experimental geometry and broad ranges of thermal parameters – has effectively bounded the real error curves. This provides a useful tool in estimating 'corrected' thermocouple temperatures, without prior knowledge of exact boundary conditions. Moreover, the bounds of this sensitivity analysis can be narrowed through further iterations after the initial correction.

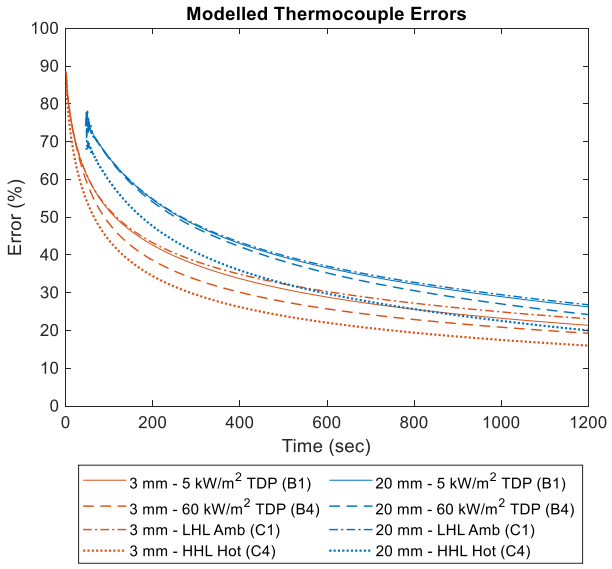

Fig. 7. Relative thermocouple errors, $E(x,t)$, calculated from tailored models with temperature-dependent properties and precisely replicated boundary conditions (B1, B4), compared with the sensitivity case models with constant material properties, an arbitrary incident heat flux, and 'low' or 'high' surface heat losses (C1, C4).

Using the simulated error histories shown in Fig. 7 and the experimentally measured thermocouple temperatures as inputs, Eq. (1) can be rearranged as shown in Eq. (8), to calculate 'corrected' thermocouple temperatures (T_{corr}), which are an estimate of the real undisturbed temperatures at the corresponding depths.

$$T_{corr}(x,t) \approx T_{un}(x,t) = \frac{(T_{\infty} \times E(x,t) - T_{TC}(x,t))}{(E(x,t) - 1)} \tag{8}$$

4.2.1 Accuracy of corrected results

These 'corrected' thermocouple results are shown in Fig. 8 a) and b). The corrected results from the tailored models with temperature-dependent properties (B1, B4) are presented as individual lines, alongside shaded areas that are bounded by the corrections calculated from the two extreme sensitivity case models (C1, C4). In general, the corrected thermocouple results provide a good approximation of the modelled undisturbed temperatures, and the corrected measurements from all of the sensitivity cases show a significant improvement on the uncorrected rear-inserted thermocouple results. The main deficiency in these model corrections is that they do not account for the effect of the moisture at lower temperatures and greater depths, as described in Section 4.1.1. This can be seen most clearly in the results of the 20 mm deep thermocouple for the 60 kW/m^2 irradiation experiment, where the corrected results significantly overestimate the real temperatures until the moisture evaporation plateau – which in reality must occur around 100 °C – has passed. The moisture effect is difficult to deal with quantitatively, since any implementation of moisture diffusion and evaporation in the model would depend on the real temperatures within the embedding material. While this could be achieved for a model with well-defined thermal properties and heating conditions, it is not feasible in the 'blind' sensitivity cases. The corrected results could be further improved if the

exact contact conditions between the thermocouple and embedding material were more accurately characterised in the model.

To illustrate the benefit of the correction, errors have been calculated for the 'corrected' results from each of the sensitivity cases, by replacing T_{TC} in Eq. (1) with the corrected temperatures T_{Corr}. In Fig. 8 c) and d), these errors are compared with those from the uncorrected experimental thermocouple results for rear-insertion, as well as the predicted error from a modelled side-inserted thermocouple (S1, S4) at a distance of 3 mm behind the heated surface. The errors calculated for the sensitivity cases have been separated into two different shaded bands based on models with ambient material properties (C1, C3), and those with hot vermiculite properties (C2, C4). These bands are delineated at their upper and lower bounds by models with high and low surface heat losses respectively. In Fig. 8 c), the calculated errors for the thermocouple 20 mm behind the heated surface were very significantly impacted by the moisture effects, so these results have been presented only from the end of the moisture evaporation plateau at 400 seconds. The calculated errors for the 20 mm thermocouples in the 5 kW/m^2 heating case, presented in Fig. 8 d), are very unstable before 150 seconds, since the temperature rise in this period is so small. Any errors prior to this time are of no real significance and have not been presented.

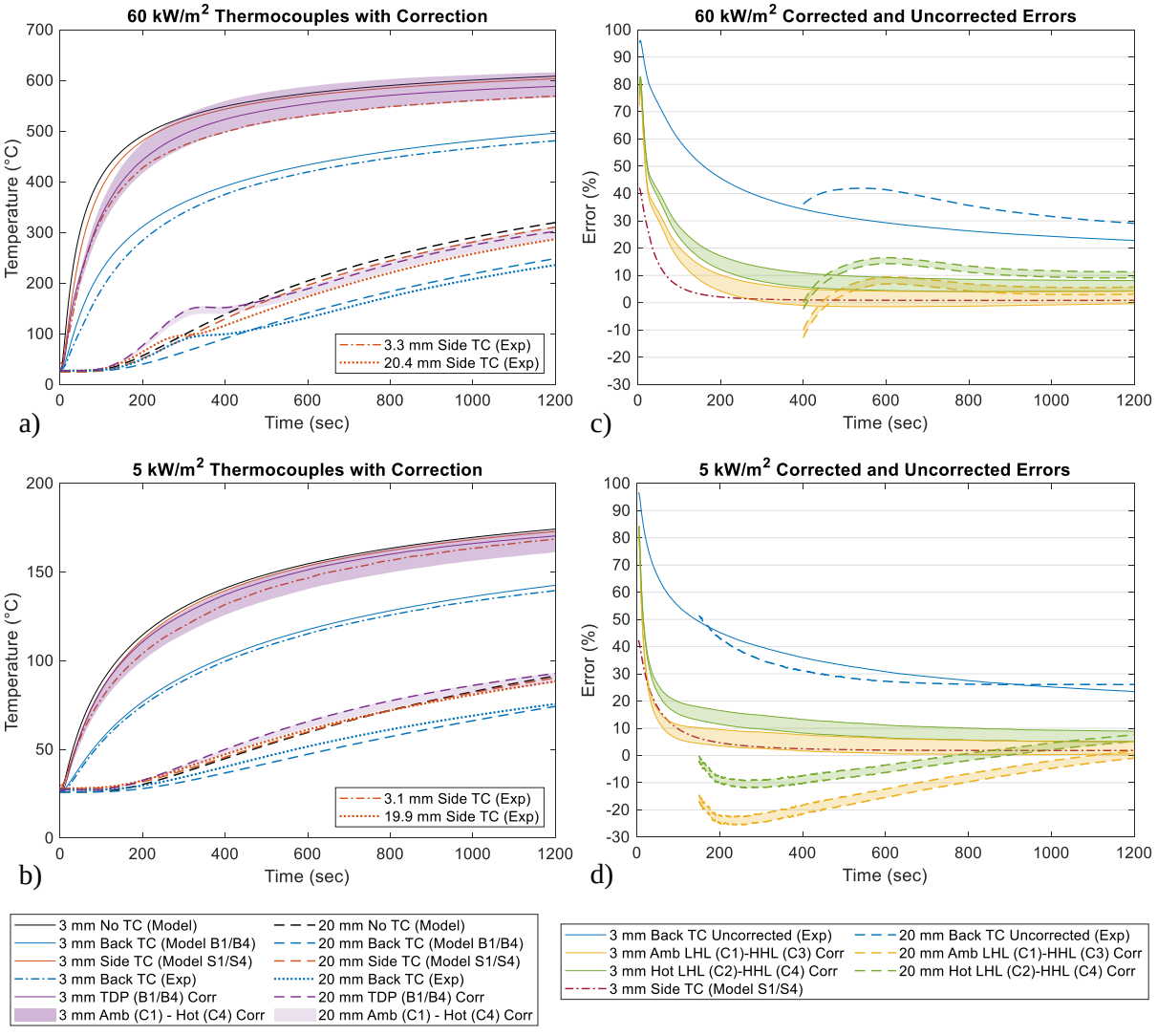

Fig. 8. Comparison between corrected and uncorrected thermocouple measurements for a) 60 kW/m^2 and b) 5 kW/m^2, and the corresponding errors calculated for 'corrected' and uncorrected measurements in c) and d). The shaded areas are bounded by the sensitivity cases C1, C2, C3, and C4.

The corrected results for rear-inserted thermocouples from all of the modelled sensitivity cases show a significant reduction in error over the uncorrected experimental measurements for all times, apart from the periods when the effects of the moisture are most dominant. Relative errors are still quite large when the heat wave first reaches each depth, but this corresponds with only small absolute differences in temperature at these times. As shown in Fig. 8 c) and d), this high early error is also apparent in the model predictions for side-inserted thermocouples. This suggests that the corrected rear-inserted thermocouple results are of comparable value even before potential tip positioning errors in the side-inserted thermocouples are considered.

As a means of comparing the value of the correction method, the route-mean-square (RMS) errors of the 'corrected' results from each case (B1/B4, C1, C2, C3, C4) have been calculated over the periods shown in Fig. 8 c) and d). These errors are shown in Fig. 9, along with the errors calculated for uncorrected experimental measurements, and for the uncorrected temperatures predicted by the tailored models (B1/B4). The corrected results, which all apply to a thermocouple of 1.5 mm diameter, are also compared with uncorrected model predictions for a 0.5 mm diameter thermocouple in a 1.0 mm hole (B9/B11). From this comparison, it is apparent that the corrections made from the 'blind' sensitivity case models still provide comparable accuracy to the corrections from the tailored models with real surface heat fluxes and temperature-dependent properties. Moreover, these corrections are also an improvement on the expected accuracy of an uncorrected 0.5 mm thermocouple, although this may not always be the case when heat transfer through the material is not solely governed by inert conduction – e.g. when moisture effects dominate.

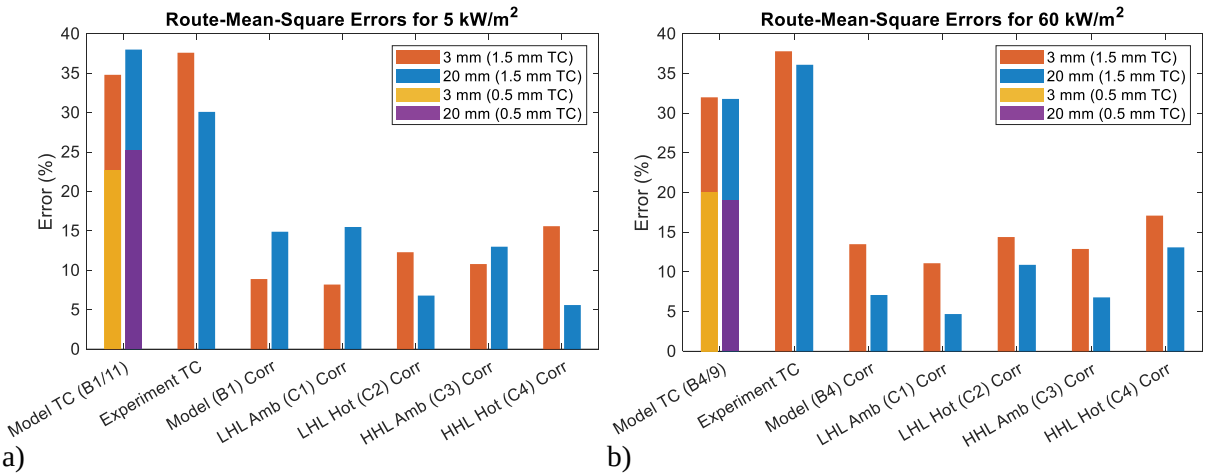

Fig. 9. Comparison of RMS errors for corrected and uncorrected modelled and experimental temperatures measured with a rear-inserted thermocouple of either 0.5 or 1.5 mm diameter. For the 20 mm depth, the RMS error is calculated for the truncated periods as shown in Fig. 8 c) and d).

4.2.2 Summary of correction process and limitations

The analysis in Section 4.2.1 has shown how relatively simple finite element modelling, based on 'blind' sensitivity cases with only minimal knowledge of thermal properties and heating conditions, can be used to calculate corrected temperature measurements within accurate ranges. This method could be applied to other experimental scenarios in which thermal properties and exposure conditions are not previously well-established. For a new material 'X', subjected to an unknown heat load, this process would be as follows:

1. Construct a heat transfer model that replicates the geometry and estimated contact conditions of each thermocouple embedded within material X, as well as the boundary conditions of the unexposed surfaces.
2. Estimate values for thermal properties that correspond to the extreme temperature conditions that could be reached.
3. Create model sensitivity cases that assign different combinations of the extreme thermal properties to each of the embedding material and the thermocouple components. These cases should encompass the highest and lowest expected values for the conductivity ratio, *K*, and the heat capacity ratio, *C*.
4. Impose a constant arbitrary surface heat flux for the period over which continuous heating is observed from the uncorrected measurements.
5. For each sensitivity case, apply a range of surface heat loss coefficients that correspond to estimated ambient and high surface temperature heat losses.
6. For each model, calculate the error history, $E(x,t)$, from the simulated thermocouple and undisturbed temperatures.
7. Use the error history calculated from the simulated temperatures for each sensitivity case to 'correct' the experimentally measured thermocouple temperatures, by modifying Eq. (1) as shown in Eq. (8). When combined, this will produce a range of corrected measurements that can be further narrowed iteratively by adjusting the bounds of the sensitivity cases as appropriate.

While potentially useful in many experimental scenarios, this method does have some limitations to its applicability and accuracy under certain conditions. Considering that the proposed models are based on heat diffusion purely through inert conduction within the solid phase, any transient effects related to the presence or migration of moisture within a porous solid will not be accounted for. As demonstrated in this study, these effects can reduce the accuracy of the 'corrected' measurements, particularly during the period before measured temperatures exceed 100 °C. This is especially troublesome under conditions where there is a significant plateau in temperatures due to moisture evaporation. Furthermore, this method is applicable for scenarios involving continuous heating, and may need to be adjusted to apply to any cooling periods. These correction models are also invalid if the geometry or contact conditions of the material around the thermocouple are altered due to behaviours such as charring, shrinkage, intumescence or delamination. However, the presence of these phenomena ahead of the thermocouple tip may be permissible, since the relative error is insensitive to the magnitude of the exposure heat flux. The precision of the range of corrected temperatures also depends on how greatly the thermal properties of the embedding material change with temperature. If these properties vary significantly, such that *K* or *C* are very different between individual sensitivity cases, the correction range will become much broader.

5. Conclusions

This study has presented the results of a sensitivity analysis of key factors influencing the thermal disturbance induced by a thermocouple in a material of lower conductivity. A series of heat transfer models and accompanying experiments demonstrated the effects of thermocouple geometry, contact conditions, thermal properties, and heat flux on the temperature measurement error. These tailored finite element models were confronted with experiments on vermiculite insulation board, which confirmed the accuracy of the models in simulating the thermal disturbance for inert heating conditions. Important outcomes of this work are that:

- The results clearly illustrate the thermal bridging effect created by a thermocouple inserted perpendicular to the heated surface of a solid. This causes a drop in temperature around the tip of the thermocouple, such that the measured temperature is much lower than the undisturbed temperature that would occur without the presence of a thermocouple.
- This error can be very large in the early heating period, exceeding 70 % of the undisturbed temperature rise, and may remain significant even as a quasi-steady state is approached.
- The disturbance is greatly reduced when the thermocouple is inserted parallel to the heated surface, but this configuration is often unfeasible in practice. Even when thermocouples can be inserted from the 'side', care must be taken to account for misplacement of the tip or movement due to shrinking or swelling of the substrate.
- Reducing the diameter of the thermocouple can also minimise the thermal disturbance, but it may still be significant even for a diameter of 0.5 mm.

Regarding temperature correction:

- A simplified version of the finite-element model was used to calculate the thermal disturbance error for a number of sensitivity cases, and subsequently to predict a range of corrected temperatures from the experimental measurements. This process requires minimal knowledge of external boundary conditions or thermal properties of the substrate, which are both varied within representative ranges.
- This correction method is simpler than Beck's [10], in that it forgoes the inverse convolution procedure to calculate correction kernels. However, like Beck's method, it can only account for inert heat diffusion between the thermocouple and surrounding material. As a result, the correction is only applicable until more complex phenomena reach the depth of the thermocouple.
- Moisture migration and accumulation under heating may be particularly problematic, because these can have a significant impact on the heat transfer even at relatively low temperatures.
- Nonetheless, when applied to the measurements of 1.5 mm diameter thermocouples inserted perpendicular to the heated surface, the corrected temperature ranges predicted through this method were a considerable improvement on the experimental measurements. These corrected temperatures had greater accuracy than even a 0.5 mm diameter thermocouple, and were comparable to the measurements from a thermocouple inserted parallel to the heated surface.
- The success of this method for the relatively simple vermiculite board provides a basis for its application to more complex materials in future studies.

Acknowledgements

The authors would like to thank the Worshipful Company of Engineers for their financial support, provided through the Sir Peter Gadsden Britain Australia Travel Award 2018. The authors are also grateful for the assistance of Jeronimo Carrascal, Michal Krajcovic and the UQ and Edinburgh fire research groups.

References

[1] P. Reszka, In-Depth Temperature Profiles in Pyrolyzing Wood, The University of Edinburgh, 2008. http://hdl.handle.net/1842/2602.

[2] F. Richter, G. Rein, A multiscale model of wood pyrolysis in fire to study the roles of chemistry and heat transfer at the mesoscale, Combustion and Flame. 216 (2020) 316–325. https://doi.org/10.1016/j.combustflame.2020.02.029.

[3] J.P. Hidalgo-Medina, Performance-Based Methodology for the Fire Safe Design of Insulation Materials in Energy Efficient Buildings, PhD Thesis, The University of Edinburgh, 2015.

[4] A. Lucherini, Fundamentals of thin intumescent coatings for the design of fire-safe structures, PhD Thesis, The University of Queensland, 2020. https://doi.org/10.14264/uql.2020.1021.

[5] CEN, Fire Resistance Tests - Part 1: General Requirements, European Committee for Standardisation, Brussels, 2012.

[6] ABCB, NCC 2019 Building Code of Australia - Volume One, Australian Building Codes Board, Canberra, 2019.

[7] G.M. Soret, D. Lázaro, J. Carrascal, D. Alvear, M. Aitchison, J.L. Torero, Thermal characterization of building assemblies by means of transient data assimilation, Energy and Buildings. 155 (2017) 128–142. https://doi.org/10.1016/j.enbuild.2017.08.073.

[8] C. Maluk, Development and application of a novel test method for studying the fire behaviour of CFRP prestressed concrete structural elements, PhD Thesis, The University of Edinburgh, 2014.

[9] T. Laschütza, Numerical and experimental investigation of a Thin Skin Calorimeter (TSC), Master's Thesis, The University of Edinburgh, 2017.

[10] J.V. Beck, Thermocouple temperature disturbances in low conductivity materials, Journal of Heat Transfer. 84 (1962) 124–131. https://doi.org/10.1115/1.3684310.

[11] R. Fahrni, J. Schmid, M. Klippel, A. Frangi, Correct temperature measurements in fire exposed wood, in: WCTE 2018 - World Conference on Timber Engineering, Seoul, Republic of Korea, 2018.

[12] I. Pope, J.P. Hidalgo, J.L. Torero, A correction method for thermal disturbances induced by thermocouples in a low-conductivity charring material, Fire Safety Journal. 120 (2021) 103077. https://doi.org/10.1016/j.firesaf.2020.103077.

[13] J.W. Woolley, K.A. Woodbury, Thermocouple data in the inverse heat conduction problem, Heat Transfer Engineering. 32 (2011) 811–825. https://doi.org/10.1080/01457632.2011.525468.

[14] D. Li, M.A. Wells, Effect of subsurface thermocouple installation on the discrepancy of the measured thermal history and predicted surface heat flux during a quench operation, Metallurgical and Materials Transactions B: Process Metallurgy and Materials Processing Science. 36 (2005) 343–354. https://doi.org/10.1007/s11663-005-0064-6.

[15] J.V. Beck, Determination of undisturbed temperatures from thermocouple measurements using correction kernels, Nuclear Engineering and Design. 7 (1968) 9–12.

[16] D. Dauti, A. Tengattini, S. Dal Pont, N. Toropovs, M. Briffaut, B. Weber, Analysis of moisture migration in concrete at high temperature through in-situ neutron tomography, Cement and Concrete Research. 111 (2018) 41–55. https://doi.org/10.1016/j.cemconres.2018.06.010.

[17] T. Arends, A.J. Barakat, L. Pel, Moisture transport in pine wood during one-sided heating studied by NMR, Experimental Thermal and Fluid Science. 99 (2018) 259–271. https://doi.org/10.1016/j.expthermflusci.2018.08.004.

[18] L. Shen, F. Lo Monte, G. Di Luzio, G. Cusatis, W. Li, R. Felicetti, F. Lombardi, M. Lualdi, M. Cao, Q. Ren, On the moisture migration of concrete subject to high temperature with

different heating rates, Cement and Concrete Research. 146 (2021) 106492. https://doi.org/10.1016/j.cemconres.2021.106492.
[19] T. Harmathy, Effect of Moisture on the Fire Endurance of Building Elements, in: A. Robertson (Ed.), Moisture in Materials in Relation to Fire Tests, ASTM International, West Conshohocken, PA, 1965: pp. 74–95.
[20] R.C. Pfahl Jr, D. Dropkin, Thermocouple Temperature Perturbations in Low-Conductivity Materials, American Society of Mechanical Engineers - Papers. Paper 66-W (1966).
[21] L. Terrei, Z. Acem, V. Marchetti, P. Lardet, P. Boulet, G. Parent, In-depth wood temperature measurement using embedded thin wire thermocouples in cone calorimeter tests, International Journal of Thermal Sciences. 162 (2021). https://doi.org/10.1016/j.ijthermalsci.2020.106686.
[22] ISO, Fire Tests Reaction to Fire Part 1: Rate of Heat Release from Building Products (Cone Calorimeter Method), International Organization for Standardization, Geneva, 1993.
[23] Special Metals Corporation, INCONEL alloy 600, (2008). http://www.specialmetals.com/assets/smc/documents/alloys/inconel/inconel-alloy-600.pdf (accessed July 15, 2019).
[24] B. Sundqvist, Thermal diffusivity and thermal conductivity of Chromel, Alumel, and Constantan in the range 100–450 K, Journal of Applied Physics. 72 (1992) 539–545. https://doi.org/10.1063/1.351885.
[25] R.W. Powell, C.Y. Ho, Liley, P E, Thermal conductivity of selected materials, U.S. Department of Commerce - National Bureau of Standards, 1966.
[26] National Institute of Standards and Technology, Magnesium oxide, (2018). https://webbook.nist.gov/cgi/inchi?ID=C1309484&Type=JANAFS&Plot=on (accessed July 15, 2019).
[27] H.W. Godbee, W.T. Ziegler, Thermal conductivities of MgO, Al2O3, and ZrO 2 powders to 850°C. I. Experimental, Journal of Applied Physics. 37 (1966) 40–55. https://doi.org/10.1063/1.1707849.
[28] F.P. Incropera, D.P. DeWitt, T.L. Bergman, A.S. Lavine, Fundamentals of Heat and Mass Transfer, 6th ed., John Wiley & Sons, Hoboken, NJ, 2007.
[29] S.W. Churchill, H.H.S. Chu, Correlating equations for laminar and turbulent free convection from a vertical plate, International Journal of Heat and Mass Transfer. 18 (1975) 1323–1329. https://doi.org/10.1016/0017-9310(75)90243-4.
[30] J.P. Hidalgo, C. Maluk, A. Cowlard, C. Abecassis-Empis, M. Krajcovic, J.L. Torero, A Thin Skin Calorimeter (TSC) for quantifying irradiation during large-scale fire testing, International Journal of Thermal Sciences. 112 (2017) 383–394. https://doi.org/10.1016/j.ijthermalsci.2016.10.013.
[31] S.W. Churchill, H.H.S. Chu, Correlating equations for laminar and turbulent free convection from a horizontal cylinder, International Journal of Heat and Mass Transfer. 18 (1975) 1049–1053.
[32] P. Boulet, G. Parent, Z. Acem, A. Collin, M. Försth, N. Bal, G. Rein, J. Torero, Radiation emission from a heating coil or a halogen lamp on a semitransparent sample, International Journal of Thermal Sciences. 77 (2014) 223–232. https://doi.org/10.1016/j.ijthermalsci.2013.11.006.